PIXL MULTISPECTRAL IMAGING: FALSE-COLOR IMAGING AND IRON-BEARING MINERAL DETECTION. D.A.K. Pedersen[1], J. Henneke[1], J.L. Jørgensen[1], Y. Liu[2], J.A. Hurowitz[3], and A.C. Allwood[2], and the PIXL team., [1]Danish Technical University, Lyngby, Denmark. (dakp@space.dtu.dk) [2]NASA-Jet Propulsion Laboratory, 4800 Oak Grove Drive, Pasadena, CA, USA. (yang.liu@jpl.nasa.gov) [3]Department of Geosciences, Stony Brook University, Stony Brook, NY, USA.

Introduction: PIXL, the Planetary Instrument for X-ray Lithochemistry, on NASA's *Perseverance* rover aims to provide a detailed geochemical assessment of past environments, habitability, biosignature preservation, and potential chemical biosignatures through texturally correlated analyses of elemental chemistry at a sub-millimeter scale [1, 2]. The PIXL sensor assembly on the robotic arm contains an optical fiducial system (OFS) that offers many key functions for PIXL measurements, including providing context to X-ray measurements, initial approach to the target, navigation of PIXL sensor head to a location specified by the operations team, achievement and maintenance of optimal X-ray focus, tracking and compensation of rover/arm thermal drifts and settling, and interpretation of X-ray spectra by providing accurate knowledge of the distance and topography of the target. Here we present additional capabilities of OFS that encompass multispectral imaging and detection of iron-bearing minerals.

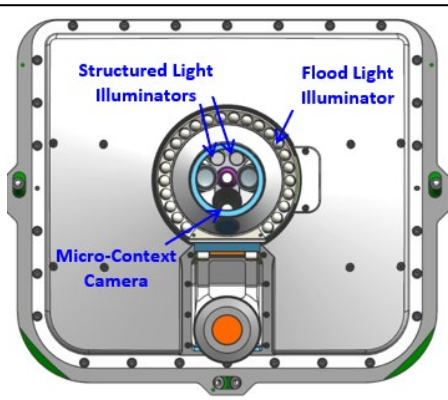

Fig. 1: The PIXL Optical Fiducial System (OFS): flood light illuminators (FLIs), structured light illuminators (SLIs), and micro-context camera (MCC).

PIXL OFS description: Arrangement of OFS components in PIXL sensor head is shown in Figure 1, including micro-context camera (MCC), floodlight illuminator (FLI), structured light illuminators (SLIs), and associated electronics. MCC contains an 8-bit grayscale CCD with a field of view of ~39 mm x 31 mm and provides a surface resolution of 70 µm when the target is in the X-ray beam focus (about 25.5 mm away from the instrument front). Two SLIs project infrared laser dots of 3x5 (dense) and 7x7 (sparse) dot patterns, respectively. With synchronized integration of the MCC's CCD and flashing of a SLI, 3D coordinates of the SLI spots are obtained, providing distance and topography information of the target, accurate to about 50 µm [1,3]. The FLI consist of an array of 24 LEDs with four channels (red, 735 nm; green, 530 nm; blue, 450 nm, and ultraviolet, 385 nm). Each LED color channel can be turned on individually to provide monochrome illumination or can be combined to provide either white or different combined colors (e.g., red + green).

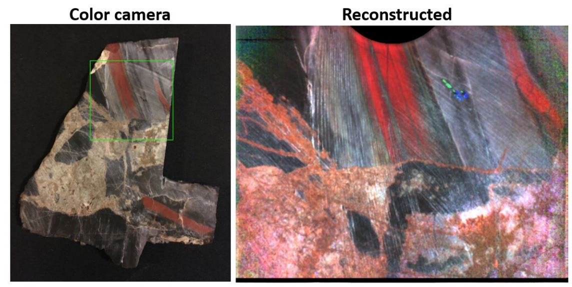

Fig. 2: A Strelly Pool rock with chert (gray and black), jasper (red) and carbonate (beige). Left: the image was taken with a standard hand-held color camera. Right: false color image was composed from the OFS raw images. Green and blue are artifacts due to spectral reflectance. Field of view on the right is 39 mm x 31 mm.

Calibration: The radiometric calibration of the FLI was performed both at the Danish Technical University during pre-delivery performance tests and at Jet Propulsion Laboratory during ATLO. Radiometric and flat-field correction schemes were developed using a radiometric calibration profile using a target with Lambertian reflectance and a flat spectral response.

Multispectral imaging: Raw monochrome images are captured for each of the four channels and merged into a composed RGB image. Each monochrome image is individually processed for radiometric corrections including flat-fielding and spectral equalization. The radiometric correction requires the 3D position information determined from the MCC-SLIs measurement. Validation of the color imaging process is shown in Figure 2.

Iron-bearing mineral detection: Reactions of the target to the monochrome LED illuminations, captured by MCC, can be potentially used to identify different iron-bearing minerals and distinguish iron-bearing from iron-free minerals. Figure 3 shows the locations of LED color channels relative to the reflectance spectra of different minerals. Iron-free minerals reflect all wavelengths equally, whereas Fe^{2+}-rich minerals (e.g, magnetite and pyrite) tend to absorb all four wavelengths equally. Fe^{3+}-bearing minerals tend to absorb the light at short wavelengths so that the spectral band ratios are sufficiently distinguishable. Example results are shown in Figure 4. The spectral ratios of all pixels (heat maps) show a mixing trend between iron-free and siderite in the carbonate conglomerate and a trend between iron-free and hematite in the banded iron formation.

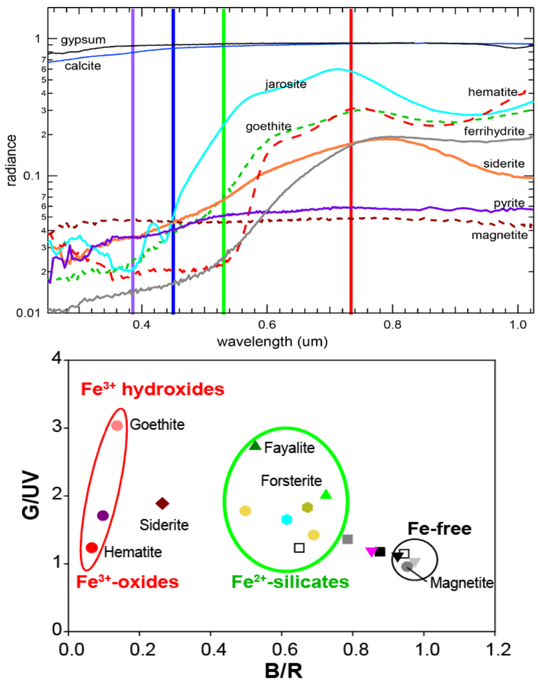

Fig. 3: Top: the OFS spectral channels with respect to mineral spectra from the USGS spectral library [4]. Bottom: mineral index based on spectral ratios.

Some ambiguities are present in using MCC color imaging to identify different iron-bearing minerals. For example, iron-free minerals, iron sulfides, and magnetite all display spectral ratios of ~1. Such ambiguities can be resolved using the color in the RGB composed image (e.g., iron-free minerals are white) and registered elemental maps from X-ray analyses (e.g., presence of sulfur for sulfides). A caveat using mineral indexes in Figure 3 is spectral responses of crystalline grains may differ from powdered samples used in the spectral library. Additional tests are underway to improve on mineral identification.

Summary: Multispectral imaging and its application to rudimental mineral detection by PIXL OFS provide important information for accurate chemical quantification by PIXL [5], such as recognizing the presence of Fe^{3+} for calculating the correct abundances of iron oxides. Besides, PIXL imaging at a higher spatial resolution in the rover arm workspace complements the multispectral analyses by Mastcam-Z at a larger scale [6].

References: [1] Allwood A.C., et al. (2020) *SSR, 216,* Article #134. [2] Allwood A.C., et al. (2021) *LPSC 52*. [3] Pedersen D. A. K. et al (2019) IEEE, TAES, 55, 4. [4] Kokaly, R. F. et al. USGS Spectral Library Version 7. Report No. 1035, 68 (Reston, VA, 2017). [5] Heirwegh, C.M., et al. (2020) LPSC 52. [6] Hayes, A.G., et al. (2020) *SSR, 216.*

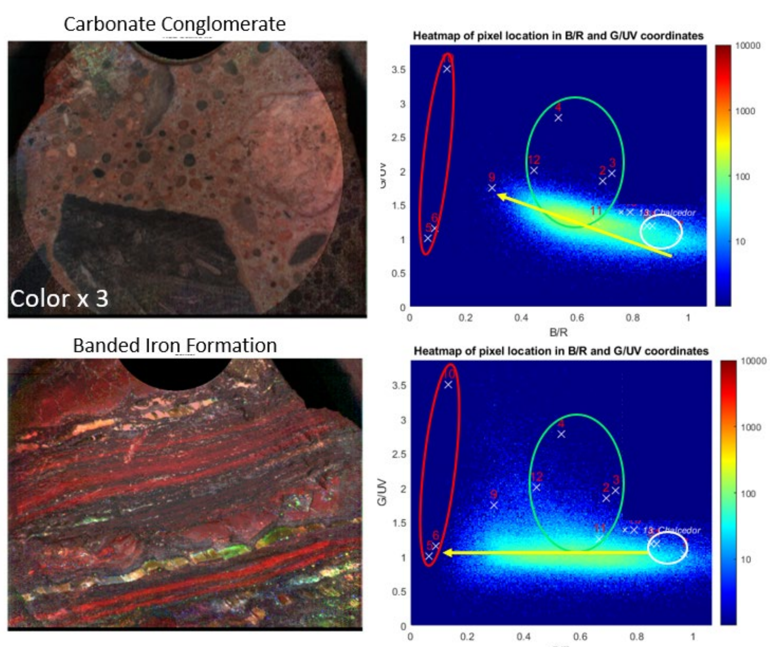

Fig. 4: False color images and mineral heat maps of a carbonate conglomerate and a banded iron formation. Yellow arrows show data trends between iron-free and siderite (top) and hematite (bottom), respectively. Ellipses on the heat maps are in the same location as those shown on Figure 3.